

DRAFT IHTC14-23100

SIMULATION OF SUB-MICRON THERMAL TRANSPORT IN A MOSFET USING A HYBRID FOURIER-BTE MODEL

James M. Loy
Purdue University
West Lafayette, IN, USA

Dhruv Singh
Purdue University
West Lafayette, IN, USA

Jayathi Y. Murthy
Purdue University
West Lafayette, IN, USA

ABSTRACT

Self-heating has emerged as a critical bottleneck to scaling in modern transistors. In simulating heat conduction in these devices, it is important to account for the granularity of phonon transport since electron-phonon scattering occurs preferentially to select phonon groups. However, a complete accounting for phonon dispersion, polarization and scattering is very expensive if the Boltzmann transport equation (BTE) is used. Moreover, difficulties with convergence are encountered when the phonon Knudsen number becomes small. In this paper we simulate a two-dimensional bulk MOSFET hotspot problem using a partially-implicit hybrid BTE-Fourier solver which is significantly less expensive than a full BTE solution, and which shows excellent convergence characteristics. Volumetric heat generation from electron-phonon collisions is taken from a Monte Carlo simulation of electron transport and serves as a heat source term in the governing transport equations. The hybrid solver is shown to perform well in this highly non-equilibrium situation, matching the solutions obtained from a pure all-BTE solution, but at significantly lower computational cost. The paper establishes that this new model and solution methodology are viable for the simulation of thermal transport in other emerging transistor designs and in other nanotechnology applications as well.

INTRODUCTION

Over the last two decades, thermal management has emerged as a critical bottleneck to the continued scaling of microelectronics [1,2]. The move to finFETs and thin-body multigate devices has led to improved sub-threshold slopes, but at the cost of increased thermal resistance [3]. Despite reduction in operating voltage, power density has been shown to scale inversely with channel length, leading to strongly non-equilibrium transport in emerging ultrascaled microelectronic devices.

Heat generated by electron-phonon scattering in the channel region of the transistor is transported to the surroundings through a cascade of thermal resistances related to the packaging design; the magnitude and arrangement of these

thermal resistances determine the mean temperature of the device. Local heating and the formation of local hot spots in the channel is, however, determined by the details of electron-phonon scattering and the rate of transport of heat by phonons at the sub-micron scale. Careful modeling of non-equilibrium transport is necessary to capture the pathways for thermal transport in these devices.

A number of research studies have demonstrated that electron-phonon scattering results in the transfer of energy to selected phonon groups [4-7] in ultra-scaled devices. Though the details of the specific phonon generation rates depend on the underlying deformation potentials, a large proportion of energy is found to be transferred to slow-moving longitudinal-optical (LO) and transverse optical (TO) phonons, and to high-frequency acoustic phonons at the edge of the Brillouin zone. The predicted rise in lattice energy (temperature) depends strongly on the group velocity of the phonons receiving the scattered energy and the rate at which they scatter energy to other phonon groups, especially fast-moving acoustic phonon groups which can transport heat to the boundaries of the device. The decay of *g*-type LO phonons has been postulated to be a rate-limiting step in silicon devices, and detailed mechanisms for their decay have been presented in [3,7,8].

Efforts to model thermal transport in ultra-scaled devices must account for these complex transport and scattering pathways. When the system length scale is comparable to or smaller than the phonon mean free path but larger than the phonon wavelength, phonon wave effects and phase coherence effects may be ignored, and phonons may be adequately described as classical particles using the phonon Boltzmann transport equation (BTE). Early work using the BTE was based on a gray description of phonons, with no accounting for phonon polarization or dispersion ([9], for example), or through two-temperature models, dividing phonons into propagating and capacitative groups [10]. More recently, more complex models accounting for phonon dispersion and polarization [11] and detailed modeling of three-phonon processes have been proposed [12-14]. Electro-thermal simulations in MOSFETs have recently been published in [3]

[15]. Here, the self-heating term is computed from an electron Monte Carlo simulation and included in a split-flux model for phonon transport; the hot spot region is solved using a ballistic BTE while the rest of the device thermal field is solved using a diffusion model. One-way coupling between a non-gray description of phonon transport and an electron Monte Carlo simulation has also been published in [14].

It has long been known that standard sequential solution techniques for the BTE and related equations in other fields, such as the radiative transport equation (RTE), are extremely slow to converge when the Knudsen number ($v\tau/L$) becomes small [16,17]. For non-gray phonon transport in silicon, for example, single-mode relaxation times have been shown to range over 3 or more orders of magnitude [18,19], so that some phonon bands are acoustically very thin, while others are very thick even in nanoscale domains. Significant convergence difficulties are encountered, and thousands of iterations may be required to obtain solutions if this range of band-wise Knudsen numbers is admitted. Furthermore, non-gray phonon transport simulations are computationally intensive. Adequate resolution of the physical and temporal domains, reciprocal space and polarization makes the computational problem nearly intractable in three dimensions. A variety of solution acceleration techniques for neutron transport and for the radiative transfer equation have been published [16,17,20-23]. However, these have not thus far been applied to the BTE. Unless these issues are resolved, non-gray solutions of complex non-equilibrium phonon transport problems will remain beyond the reach of available computational power.

In [24], we developed a novel hybrid Fourier-BTE model for phonon transport which addresses both the issues of solution acceleration and computational effort. Here, phonons are divided into bands, each corresponding to a particular range of frequency, and belonging to a specific polarization. Phonon bands with band-wise Knudsen numbers below a chosen cutoff are described by modified Fourier equations for the band "temperature," accounting for inter-band phonon-phonon scattering and wall slip. Those bands with Knudsen numbers greater than the cutoff are represented by non-gray BTEs. Because the BTE bands are thin, convergence issues associated with low Knudsen numbers are not encountered. A block-coupled solution procedure is used to address inter-band coupling inexpensively for the Fourier bands. The resulting algorithm has been shown to be 3-100 times faster than an all-BTE solution procedure, with little loss of accuracy.

In this paper, we apply our hybrid Fourier-BTE model to the prediction of the thermal field in a bulk MOSFET. One-way coupling with an electron Monte Carlo solver [6] is used to provide the Joule heating source term, which is resolved in terms of phonon polarization and wave vector. A non-gray description of phonon transport forms the basis of our hybrid model. In the sections that follow, we first present an overview of the hybrid model and the computational scheme. The MOSFET model and heat source computation are described, Results for the temperature field and heat flux distributions

obtained by the hybrid model are compared to those obtained using an all-BTE model, and shown to compare well. Results for CPU time and iterations to convergence for both models are also presented, and the advantages of the hybrid Fourier-BTE model for MOSFET simulation are established.

NOMENCLATURE

C	phonon specific heat [J/m^3K]
e^0	average spectral energy density [J/m^3sr]
e''	spectral energy density [J/m^3sr]
\bar{e}''	band-average specular energy density [J/m^3sr]
f^0	equilibrium phonon distribution
\hbar	Planck's constant [Js]
\mathbf{i}	unit vector in x direction
\mathbf{j}	unit vector in y direction
\mathbf{k}	unit vector in z direction
k	phonon thermal conductivity [W/mK]
K	phonon wave number [m^{-1}]
Kn	Knudsen number ($=v\tau/L$)
L	domain characteristic length [m]
\mathbf{n}	outward pointing normal unit vector
\mathbf{q}''	heat flux vector [W/m^2]
\mathbf{r}	position vector [m]
R_L	lattice ratio ($=(C/\tau)/\sum C/\tau$)
\mathbf{S}	phonon direction unit vector
T	temperature
T_L	lattice temperature [K]
T_{ref}	reference temperature [K]
v	phonon group velocity [m/s]
x, y	coordinate directions
x^*, y^*	dimensionless coordinates $x/L, y/L$

Greek

$\Delta\Omega$	solid angle control volume [sr]
θ	polar angle [rad]
φ	azimuthal angle [rad]
Φ	band energy perturbation [J/m^3sr]
ω	phonon frequency [rad/s]

Subscripts

L	relating to the lattice temperature
p	phonon polarization
$wall$	relating to a wall boundary
ω	phonon frequency [rad/s]

HYBRID FOURIER-BTE MODEL

In the hybrid model, the phonon spectrum is divided into frequency bands with frequencies ω and polarization p , as shown in Fig. 1.

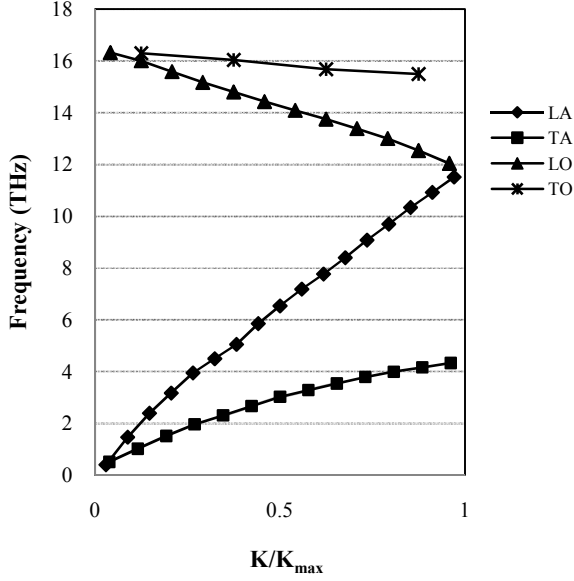


Figure 1: Discretized phonon dispersion for phonon modes.

Each band is characterized by a band specific heat $C_{\omega,p}$, group velocity vector $\mathbf{v}_{\omega,p}$ and relaxation time $\tau_{\omega,p}$. In this paper, these quantities are computed using the dispersion curves in the [100] of silicon using the environment-dependent interatomic potential [25,26]. Each band is thus characterized by its Knudsen number

$$Kn_{\omega,p} = \frac{v_{\omega,p} \tau_{\omega,p}}{L} \quad (1)$$

and the lattice ratio

$$R_{L,\omega,p} = \frac{C_{\omega,p} / \tau_{\omega,p}}{\sum_{\omega,p} C_{\omega,p} / \tau_{\omega,p}} \quad (2)$$

A cutoff Knudsen number Kn_{cutoff} is chosen; a value of 0.1 is used in this paper. If $Kn_{\omega,p} > Kn_{cutoff}$, the band is described by a non-gray phonon BTE in the relaxation time approximation. If $Kn_{\omega,p} \leq Kn_{cutoff}$, a modified Fourier equation is used to describe the band. The band specific heat is assumed independent of temperature in this paper. This assumption is made only for clarity, and is easily relaxed in the formulation. It is strictly valid only for temperatures greater than the Debye temperature, or if temperature differences in the problem are small.

Phonon Boltzmann Transport Equation

The steady-state, non-gray BTE for a phonon band of frequency ω and polarization p under the relaxation time approximation is given in energy form by [27]:

$$\nabla \cdot (\mathbf{v}_{\omega,p} e''_{\omega,p}) = \frac{e^0_{\omega,p} - e''_{\omega,p}}{\tau_{\omega,p}} \quad (3)$$

where $e''_{\omega,p}$ is the volumetric energy density per unit solid angle at a given frequency and polarization, and $e^0_{\omega,p}$ is the corresponding equilibrium energy density given by a Bose-Einstein distribution [28]. For relatively small lattice temperature differences, and under the assumption of crystal isotropy, $e^0_{\omega,p}$ is given by

$$e^0_{\omega,p} = \frac{C_{\omega,p}}{4\pi} (T_L - T_{ref}) \quad (4)$$

Here, T_L is the lattice temperature, and is defined in a later section, and T_{ref} is a temperature that defines the energy datum. The band specific heat $C_{\omega,p}$ is given by:

$$C_{\omega,p} = \int_{\Delta K} \hbar \omega \frac{\partial f^0}{\partial T} 4\pi K^2 dK \quad (5)$$

where ΔK denotes the volume of the Brillouin zone associated with the frequency and polarization under consideration. Furthermore, the total energy associated with the band is

$$\int_{4\pi} e''_{\omega,p} d\Omega = C_{\omega,p} (T_{\omega,p} - T_{ref}) = 4\pi \bar{e}''_{\omega,p} \quad (6)$$

where $T_{\omega,p}$ is the equilibrium “band temperature” associated with the average energy density $\bar{e}''_{\omega,p}$ of the band. It has no thermodynamic meaning, and should only be construed as a measure of band energy density.

Boundary Conditions for BTE Bands

Two thermal boundary conditions are used in this paper for BTE simulations: (i) thermalizing boundaries, and (ii) diffusely reflecting boundaries.

Thermalizing boundary: For phonons going into the domain from a thermalizing boundary at temperature T_1 , the energy density of a band with frequency ω and polarization p is given by:

$$e''_{1,\omega,p} = \frac{C_{\omega,p}}{4\pi} (T_1 - T_{ref}) \quad (7a)$$

For directions outgoing from the domain, the following upwind condition is applied:

$$\nabla e''_{\omega,p} \cdot \mathbf{s} = 0 \quad (7b)$$

where \mathbf{s} is the unit vector associated with the group velocity vector outgoing to the domain.

Diffusely-reflecting boundary: Assuming elastic collisions with the boundary, the energy density of phonons leaving the boundary and entering the domain is given by [29]:

$$e''_r = e''_{\omega,p}(\mathbf{s}, \mathbf{r}) \Big|_{s \cdot \mathbf{n} < 0} = \frac{1}{\pi} \int_{s \cdot \mathbf{n} \geq 0} e''_{\omega,p} \mathbf{s} \cdot \mathbf{n} d\Omega \quad (8)$$

Here, \mathbf{n} is the outward pointing normal to the boundary. For directions outgoing to the domain, Eq. 7(b) applies.

Modified Fourier Equation

For bands with $Kn_{\omega,p} > Kn_{cutoff}$ a modified band-wise Fourier equation is developed. Eq. (3) is integrated over the solid angle 4π to obtain an expression for the heat flux vector $\mathbf{q}''_{\omega,p}$ associated with the band:

$$\nabla \cdot \mathbf{q}''_{\omega,p} = \frac{C_{\omega,p}}{\tau_{\omega,p}} (T_L - T_{\omega,p}) \quad (9)$$

For near-equilibrium situations, such as in thermal conduction, we may make the approximation

$$\nabla \cdot (\mathbf{v}_{\omega,p} e''_{\omega,p}) \approx \mathbf{v}_{\omega,p} \cdot \nabla \bar{e}''_{\omega,p} \approx C_{\omega,p} \mathbf{v}_{\omega,p} \cdot \nabla T_{\omega,p} \quad (10)$$

Multiplying Eq. (3) by $\mathbf{v}_{\omega,p}$, using the approximation in Eq. (10) and integrating over 4π yields the Fourier heat flux relationship for the band:

$$\mathbf{q}''_{\omega,p} = -k_{\omega,p} \nabla T_{\omega,p} \quad (11)$$

where the band thermal conductivity $k_{\omega,p}$ is given by

$$k_{\omega,p} = \frac{1}{3} C_{\omega,p} v_{\omega,p}^2 \tau_{\omega,p} \quad (12)$$

Combining Eqns. (9), (11) and (12) yields the Fourier equation for the band:

$$\nabla \cdot (-k_{\omega,p} \nabla T_{\omega,p}) = \frac{C_{\omega,p} (T_L - T_{\omega,p})}{\tau_{\omega,p}} \quad (13)$$

Boundary Conditions for Modified Fourier Equation

Again, two thermal boundary conditions are considered: (i) thermalizing boundaries, and (ii) diffusely reflecting boundaries.

Thermalizing boundary: The classical Fourier heat conduction is incapable of predicting temperature jumps at thermalizing boundaries. In order to capture wall temperature jumps, a first-order perturbation is employed. The energy density $e''_{\omega,p}$ is decomposed as the sum of the average energy of each band and a direction-dependent perturbation:

$$e''_{\omega,p} = \bar{e}''_{\omega,p} + \Phi_{\omega,p}(\mathbf{r}, \mathbf{s}) \quad (14)$$

Here $\Phi_{\omega,p}$ is the directionally dependent perturbation. The average band energy is defined in Eqn. (6). We insert Eqn. (14) into the BTE (Eq. 3). Furthermore, we assume that the divergence of $\Phi_{\omega,p}$ is negligible compared to the divergence of the average band energy density; this is true for low band Knudsen numbers ($Kn_{\omega,p} \leq 0.2$). By invoking Eqn. (10), we may obtain an equation for the perturbation at any spatial location for the band as:

$$\Phi_{\omega,p} = \frac{C_{\omega,p}}{4\pi} \left[(T_L - T_{ref}) - v_{\omega,p} \tau_{\omega,p} \nabla \cdot (\mathbf{s} T_{\omega,p}) \right] \quad (15)$$

The above equation adds an anti-symmetric perturbation to the average energy density. This asymmetry is responsible for creating a heat flux through the domain.

We now examine the thermalizing boundary. The energy in any band entering the domain from the boundary is assumed to be diffuse and is given by

$$e''_{1,\omega,p} = \frac{C_{\omega,p}}{4\pi} (T_1 - T_{ref}) \quad (16)$$

The average energy density at the wall is computed as an average of the incoming and outgoing energies as

$$e^0_{1,\omega,p} = \frac{1}{4\pi} \left[\int_{s \cdot \mathbf{n} < 0} e''_{1,\omega,p} d\Omega + \int_{s \cdot \mathbf{n} \geq 0} e''_{\omega,p} d\Omega \right] \\ = \frac{1}{4\pi} \left[\frac{e''_{1,\omega,p}}{2} + \frac{\bar{e}''_{\omega,p} + \Phi_{\omega,p}(\mathbf{r}, \mathbf{s})}{2} \right] \quad (17)$$

We may express the average energy density at the wall in terms of a wall temperature for the band as:

$$e^0_{1,\omega,p} = \frac{C_{\omega,p}}{4\pi} (T_{\omega,p,wall} - T_{ref}) \quad (18)$$

Performing the integration in Eq. (17), and using Eqns. (15), (16) and (18), we obtain

$$T_{\omega,p,wall} = \frac{T_1 + T_L}{2} + \frac{v_{\omega,p} \tau_{\omega,p}}{4} \nabla T_{\omega,p} \cdot \mathbf{n} \quad (19)$$

Employing Eq. (12) and re-arranging the terms, Eq. (19) may be cast as a standard Robbins boundary condition:

$$\begin{aligned} (-k_{\omega,p} \nabla T_{\omega,p}) \cdot \mathbf{n} &= AT_{\omega,p,wall} + B \\ A &= -\frac{4}{3} C_{\omega,p} v_{\omega,p} \\ B &= \frac{2C_{\omega,p} v_{\omega,p}}{3} (T_1 + T_L) \end{aligned} \quad (20)$$

Diffusely reflecting boundary: Next we must examine diffusely reflecting boundary condition. The heat flux normal to a boundary with an outward-pointing normal unit vector \mathbf{n} is given by

$$\mathbf{q}_{\omega,p}'' \cdot \mathbf{n} = \int_{4\pi} v_{\omega,p} e_{\omega,p}'' \mathbf{s} \cdot \mathbf{n} d\Omega \quad (21)$$

where the heat flux vector $\mathbf{q}_{\omega,p}''$ is given by Eq. (11). At a reflecting boundary, the heat flux may be written in terms of the energy transfers incoming to and reflected from the boundary:

$$\begin{aligned} -k_{\omega,p} \nabla T_{\omega,p} \cdot \mathbf{n} &= v_{\omega,p} \left[\int_{s \cdot \mathbf{n} < 0} e_r'' \mathbf{s} \cdot \mathbf{n} d\Omega + \int_{s \cdot \mathbf{n} \geq 0} e_{\omega,p}'' \mathbf{s} \cdot \mathbf{n} d\Omega \right] \\ &= 0 \end{aligned} \quad (22)$$

The net reflected energy (the first integral on the RHS) must be equal opposite in sign to the net incoming energy (the second integral on the RHS) yielding an adiabatic boundary condition. It is important to note that the modified Fourier equation cannot determine the difference between diffuse, partially specular, and fully-specular boundary conditions. All three yield the same boundary condition, Eq. (22).

LATTICE TEMPERATURE

The scattering terms in the BTE and the modified Fourier equations must be purely redistributive in the aggregate, and no energy may be created or lost due to scattering processes. Thus, the net scattering term, summed over all bands, must be zero:

$$\sum_{\omega,p} \frac{4\pi (e_{\omega,p}^0 - \bar{e}_{\omega,p}'')}{\tau_{\omega,p}} = 0 \quad (23)$$

Using Eqns. (4) and (6) and re-arranging, we obtain

$$T_L = \left[\sum_{\omega,p} \frac{C_{\omega,p}}{\tau_{\omega,p}} T_{\omega,p} + \sum_{\omega,p} \frac{C_{\omega,p}}{\tau_{\omega,p}} T_{\omega,p} \right] \left(\sum_{\omega,p} \frac{C_{\omega,p}}{\tau_{\omega,p}} \right)^{-1} \quad (24)$$

The first summation in the square brackets is a summation over all BTE bands, while the second summation is over all Fourier bands. The summation in the last term is over all bands, BTE and Fourier.

NUMERICAL METHOD

Discretization

A finite volume method is used to solve both the BTE and the Fourier equations [16]. The same mesh is used for both the BTE and Fourier bands. The computational domain is divided into rectangular cells or control volumes. For the BTE, we follow discretization procedures similar to those described in [30]. The BTE in any given direction for a band (ω,p) is integrated over the control volume and the solid angle to yield an energy balance statement for the control volume. For the purposes of this paper, a first-order convective operator is used, though higher-order discretizations are easily admitted. The scattering operator is discretized using a second-order operator. The modified Fourier equations are discretized using standard second-order finite volume procedures described in [31].

Solution Procedure for Hybrid Fourier-BTE Model

Under the assumption of constant specific heats, the Fourier and BTE equations are linear, a direct solution of the discretized forms of Eqns. (3), (13) and (24) may be found. However, in typical non-gray problems, there would be several tens of phonon bands, and even with a modest discretization of angular space, several hundred BTEs; the storage and CPU requirements for direct schemes would be too onerous for practical use.

Typical solution procedures published for the BTE [11,12,14,30] employ a sequential procedure whereby the BTE in each frequency band and direction is solved sequentially, assuming prevailing values for T_L in evaluating the energy density $e_{\omega,p}^0$. Such a procedure has low memory requirements, and a similar one could be employed here. We would start with a guess of the lattice temperature T_L and solve the BTE equations sequentially over the spatial domain, keeping the lattice temperature fixed at its prevailing value. Then the Fourier equations would be solved sequentially, again keeping

T_L at prevailing values. Eq. (24) would then be used to update T_L . The procedure would be repeated until convergence.

This type of sequential procedure was found to be extremely slow, and was impeded primarily by the explicit update of T_L . In typical nanoscale thermal transport problems, the structure of Eq. (24) dictates that the lattice temperature T_L is influenced most strongly by bands with a larger lattice ratio, i.e., by phonon bands with the smallest scattering times $\tau_{\omega,p}$. That is, the Fourier bands are the most strongly coupled to each other, through the lattice temperature T_L . Though the BTE bands are also coupled to each other through T_L , the strength of their coupling is proportional to $(Kn_{\omega,p})^{-1}$, which is small by design. Thus, a computational scheme which solves the Fourier bands simultaneously with Eq. (24) is likely to yield solution acceleration. Furthermore, though a direct solution of the BTE and Fourier bands together is too expensive to contemplate, a direct solution of the Fourier bands (Eq. (13)) and the lattice temperature equation (Eq. (24)), is affordable since the modified Fourier equations are direction-independent.

Following the development in [24], we employ a sequential solution of the BTE equations as before, but now augmented by a partially-implicit solution of the Fourier and lattice temperature equations (Eq. (13)) and Eq. (24)). The computation is initiated with a guess of the lattice temperature. We loop sequentially over the BTE bands keeping the lattice temperature fixed at its prevailing value. For each BTE band, the BTE in each direction is solved sequentially, sweeping over the spatial grid in the direction of the group velocity vector. Once all BTE bands have been updated, the Fourier bands (Eq. (13)) and the lattice temperature equation (Eq. (24)) are solved together, using a block-coupled line-by-line tridiagonal matrix algorithm [31]. In this coupled solution, the BTE contribution to Eq. (24) is held at prevailing values. The procedure is repeated until a prescribed convergence criterion is met.

Solution Procedure for All-BTE Computations

In the section below, comparisons of CPU time and iterations to convergence for the hybrid model are made against an all-BTE solution. For the latter approach, Eq. (3) is solved for all bands, and T_L computed using Eq. (23). A sequential procedure is employed. The procedure starts with a guess of T_L . For each BTE band, the BTE in each direction is solved sequentially, sweeping over the spatial grid in the direction of the group velocity vector. Once all BTE bands have been updated, T_L is updated using Eq. (23). The procedure is repeated until convergence.

MOSFET ELECTRO-THERMAL SIMULATION

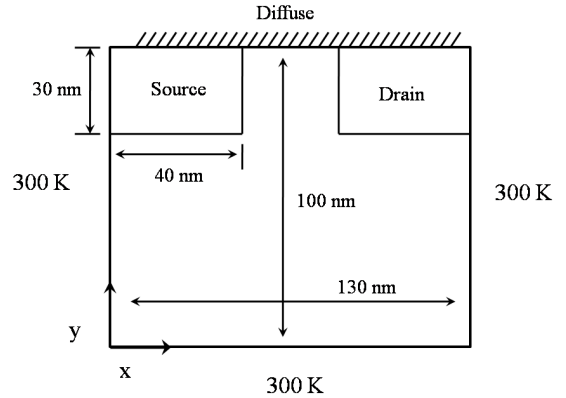


Figure 2: Schematic of domain to be solved. Adapted from [29]

Computational Domain

We now turn to the electro-thermal simulation of a bulk Si MOSFET, as shown in Fig. 2. A two-dimensional rectangular domain encompassing the source, drain, and channel regions is considered, with the dimensions shown in Fig. 2. The device is an NPN FET with source/drain doping of $1 \times 10^{20} \text{ cm}^{-3}$. The channel region of the substrate is doped to $1 \times 10^{18} \text{ cm}^{-3}$ while the rest of the substrate is doped to $1 \times 10^{16} \text{ cm}^{-3}$. The source/drain regions are $40 \text{ nm} \times 30 \text{ nm}$ in the top right and left corners, respectively, and the gate oxide is 2 nm thick. Source/drain and gate voltages are set to be 1 V .

For the purpose of thermal simulation, the left, bottom and right boundaries are assumed to be at a reference temperature of 300 K , while the top boundary is assumed diffusely reflecting. The true temperature of the left, bottom and right boundaries depends on the thermal resistance to the heat sink, and therefore, to the packaging design. In a linear model, such as that in this paper, the computed temperature differences are independent of the assumed boundary temperature, and are a measure of the degree of self-heating. Furthermore, since our goal is to compare our predictions with an all-BTE solution, the specific value of the boundary temperature is not important.

A non-uniform spatial mesh of 100×60 cells is used in all computations using the hybrid model. Mesh independence tests were performed by Ni in [29] and little change was found in the overall heat flux with a mesh of 50×30 . The same mesh is used for all-BTE calculations reported in this section. Dispersion curves for bulk silicon in the $[100]$ directions are used to determine phonon bands, as shown in Fig. 1. A total of 46 different phonon bands are used to discretize the phonon spectrum, including all polarizations. Kn_{cutoff} is chosen to be 0.1. With this cutoff, for $L = 400 \text{ nm}$, 12 bands are found to be Fourier bands, accounting for a total lattice ratio of 0.73. An angular discretization of 4×4 angles in the octant is used.

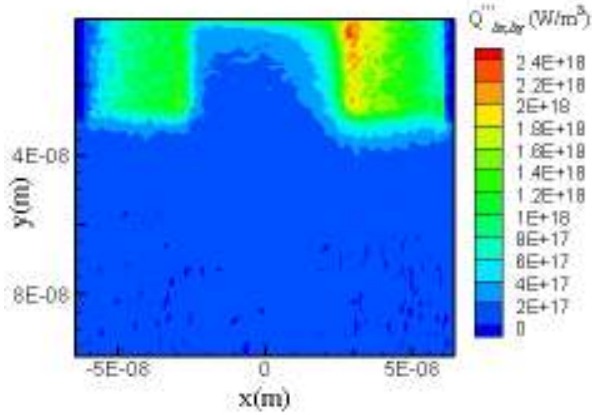


Fig. 3: Spatial distribution of heat generation due to electron-phonon scattering [29].

Table 1 .Percentage of heat generation in each phonon polarization [29].

Phonon polarization	% of Heat generation
TA1	2.0
TA2	2.4
LA	16.0
LO	59.0
TO1	10.5
TO2	10.1
Total	100

Computation of Relaxation Times

Frequency-dependent relaxation times for impurity and Umklapp scattering are taken from [32] and are given by

$$\tau_{im}^{-1} = A\omega^4$$

$$\tau_u^{-1} = B T \omega^2 e^{-C/T}$$

A , B , and C are constants equaling $1.32 \times 10^{-45} \text{ s}^3$, $1.73 \times 10^{-19} \text{ s/K}$, and 137.39 K , respectively. The parameters are found by fitting bulk thermal conductivity predicted by using these scattering rates to experimental thermal conductivity values for silicon.

Computation of Joule Heating Source Term

A one-way coupling between the electron and phonon populations is assumed. The heat generation rates for each phonon band are obtained from an electron Monte Carlo (eMC) simulation which includes full phonon dispersion [29,33]. The Monte Carlo simulation is performed in a 3D domain of $100\text{nm} \times 130\text{nm} \times 100 \text{ nm}$, and the results are averaged over the device depth to provide spatially distributed heat source terms to the phonon simulation. Details of the averaging procedure

and the post-processing of the eMC results are described in detail in [14].

The total heat added to the domain is 3197.9 W/m . Fig. 3 shows the spatial distribution of the heat source due to electron-phonon scattering, while Table 1 shows the distribution of the heat generation with respect to phonon polarization. The branches TA1 and TA2 are aggregated into a single polarization in the [100] direction in this paper, as are the TO1 and TO2 bands. As expected, the bulk of the heat generation occurs in the drain region of the device, and nearly 60% of the energy due to electron phonon scattering is transferred to the LO branch.

RESULTS AND DISCUSSION

In this section, we first present band-wise and lattice temperature computed using the hybrid model and compare them to the distributions obtained using an all-BTE simulation. Comparisons are then made of the spatial distributions of the bandwise and total heat fluxes for the two models. Finally, comparisons of the CPU time and iterations-to-convergence are presented.

Temperature

Figure 4 shows a contour plot of the lattice temperature obtained using the hybrid Fourier-BTE model. The maximum temperature rise with respect to the boundary is predicted to be 60 K. Though some heating is seen in the source region, the bulk of the self heating is seen to occur in the drain. This is consistent with the spatial distribution of the heat generation shown in Fig. 3. This shifting of hot spot location to the drain region is a direct result of electron acceleration due to the presence of high electric fields in modern MOSFETS.

Figures 5-7 show a comparison between the hybrid solver and the BTE along three different lines. The first line is at $x^*=1/6$, which is a vertical line passing through the middle of the source. The second line is at $x^*=5/6$, which is a vertical line drawn through the middle of the drain. The third line is at $y^*=0.85$, which is a horizontal line drawn through the middle of the source and drain. The temperature $T_{\omega,p}$ defined in Eq. (6), is plotted, but now accounting for the total energy associated with each polarization. As expected, the highest temperature is associated with the optical branches, with the LO and TO branches being the hottest. This is in keeping with the distribution shown in Table 1, where the LO band accounts for 59% of the heat generation while the TO branches receive 20.6% of the heat generation. Furthermore, these modes also have the lowest group velocity. The lattice temperature is seen to be closer to the optical mode temperatures because of large lattice ratio associated with these modes.

Figs. 5-7 also show a detailed comparison of the band-wise temperatures predicted by the hybrid and all-BTE simulations. The two predictions are nearly indistinguishable. The RMS error on the total domain for the lattice, LA, TA, LO and TO temperatures are 0.29%, 0.19%, 0.17%, 0.37%, and 0.32%, respectively.

The lattice temperature predictions obtained here are somewhat at variance with those in [14] for the same device, though the basic temperature distribution is similar. In [14], Ni predicted a rise of 46.5 K, while we predict a rise of 60.0 K. There are several reasons for this discrepancy. The primary difference is due to a difference in scattering rates. The scattering rates in this paper are found by assuming scattering rate expressions from [32] and fitting model constants to the bulk thermal conductivity of silicon, while those in [14] were found by enforcing three-phonon interaction rules and using perturbation theory [34]. Furthermore, [14] did not make an isotropic assumption in K-space, and the dispersion relationship was computed using a bond-charge model.

The maximum temperature rise predicted in this paper is significantly lower than those predicted in early MOSFET simulations [10]; a similar observation has also been made in [15]. The primary reason for the high temperature predictions in early papers is the lack of resolution of non-gray effects, and particularly, the assumption that optical modes were essentially stationary. Though optical mode group velocities are lower than those for acoustic modes, they are not zero, and their inclusion has been shown in [14] to substantially lower the maximum temperature prediction.

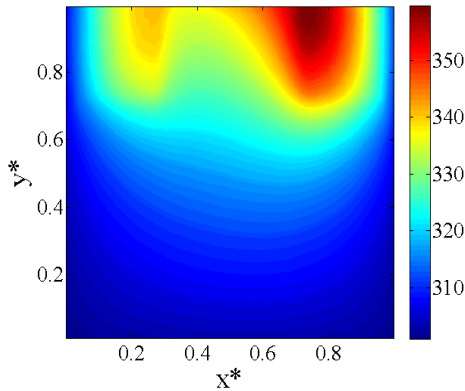


Figure 4: Contours of lattice temperature (K) calculated by the hybrid solver.

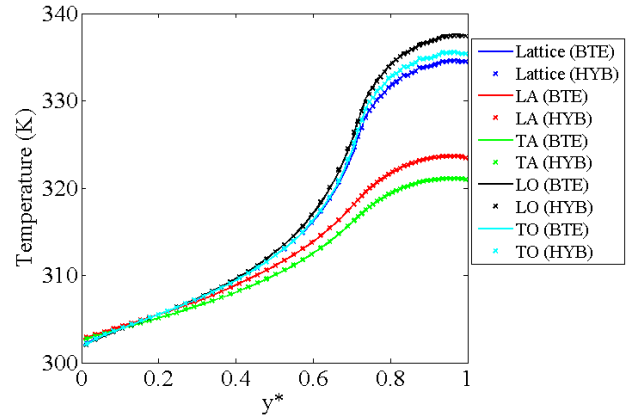


Figure 5: Temperature variation along the line $x^*=1/6$

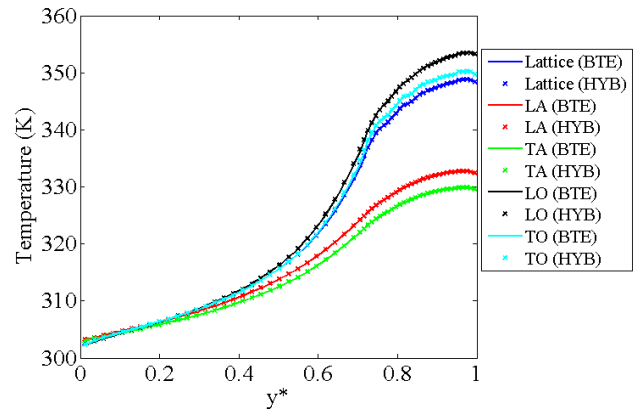


Figure 6: Temperature variation along $x^*=5/6$

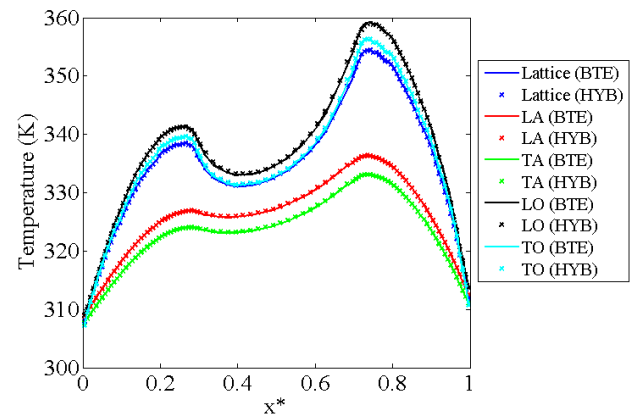


Figure 7: Temperature variation along $y^*=0.85$

Heat Flux

Figures 7-9 show the dimensionless heat flux (q''_{branch}/q''_{total}) for each polarization for the left, bottom, and right boundaries. The results obtained from the hybrid solver are compared to an all-BTE solution.

The LA modes are seen to carry most of the heat to the boundaries, as seen in Figs. 7-9, followed by the TA modes; the optical modes, despite receiving most of the heat generated due to electron-phonon scattering, are responsible for only a small fraction of the heat flux at the boundaries. This suggests that scattering from the optical to the acoustic modes is accomplished over length scales of the order of $\sim 100\text{nm}$ using the scattering rate models employed in this paper. Furthermore, for locations $y^* > 0.6$ or so in Figs. 7 and 9, the LO mode heat flux is seen to be higher than that for the TA modes. These locations are close to the hot spots in the source and drain regions, and the scattering of energy from optical to acoustic modes is not yet complete.

The global heat flux error, compared to an all BTE solution, on the left, bottom, and right boundaries are 0.41%, 0.70%, 0.51%, respectively. Table 2 shows the percentage of total heat leaving through the boundaries for each polarization. The heat flux is dominated by the high $Kn_{\omega,p}$ bands, and since these are solved using a BTE, good comparisons with the all-BTE solution are obtained. Lattice temperature profiles, on the other hand, is dominated by the Fourier bands because of their low scattering times $\tau_{\omega,p}$. Since a Fourier conduction equation is appropriate for these thick bands, the hybrid solver solution matches the all-BTE solution well.

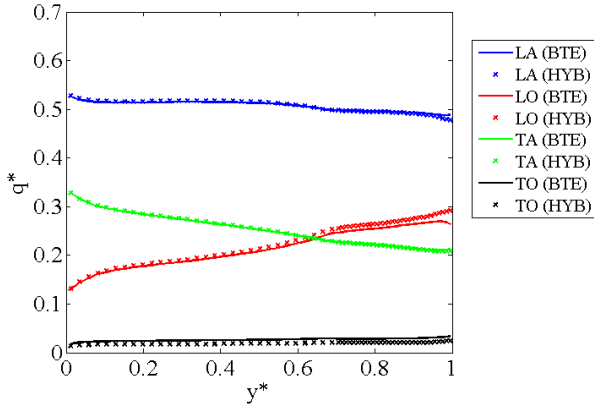


Figure 7: Dimensionless heat fluxes leaving the left boundary for both hybrid and all-BTE solvers.

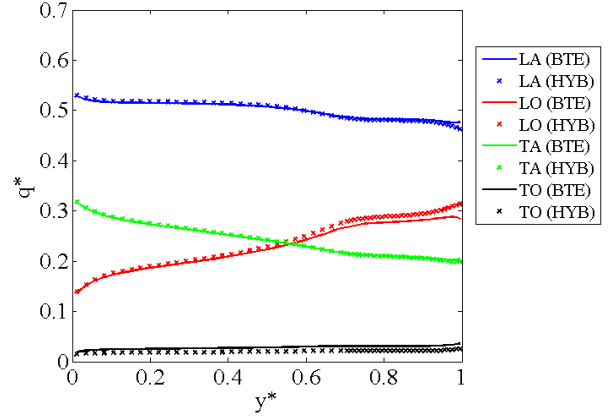


Figure 9: Dimensionless heat fluxes leaving the right boundary for both hybrid and all-BTE solvers.

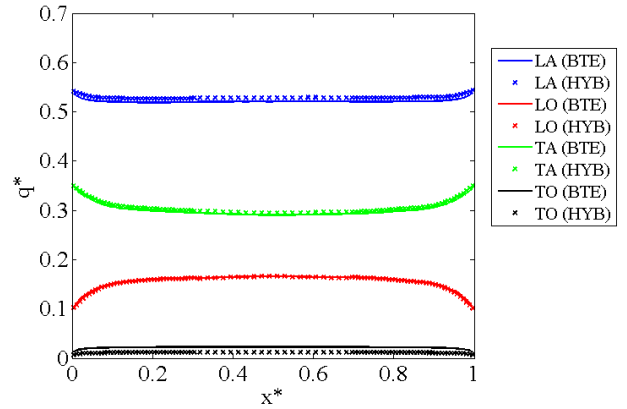


Figure 8: Dimensionless heat fluxes leaving the bottom boundary for both hybrid and all-BTE solvers.

Table 2: Percentage of total heat leaving the boundaries for each branch.

	Hybrid (%)	BTE (%)
LA	51.27	50.94
TA	27.00	26.81
LO	20.15	19.74
TO	1.57	2.51

Timing

For the all-BTE simulation, one iteration consists of the sequential solution of each phonon band, and an update of the lattice temperature. The total iteration count was 130, with a total elapsed time of 24,794.1 seconds. For the hybrid simulation, one iteration consists of the simultaneous solution of all the Fourier bands and the lattice temperature, followed by the sequential solution of each BTE band. The total iteration count was 34, with a total elapsed time of 12,671.0 seconds.

The timings reveal that though the hybrid solver is twice as fast as the all-BTE solver, there remains significant room for improvement. For each hybrid iteration, the number of equations to be solved is about $\frac{3}{4}$ the number equations in an all-BTE iteration. Therefore, we would expect the time per hybrid iteration to be roughly $\frac{3}{4}$ the time per all BTE iteration. In fact, one all-BTE iteration is found to be approximately twice as fast one hybrid iteration. This counter-intuitive result is because of the inefficiency of the line-by-line block TDMA used to solve the Fourier plus lattice equations. For fine meshes, the line Gauss-Seidel procedure results in slow convergence rates, as discussed in [35]. We still see a speed-up of about 2x because the number of iterations required for the hybrid is about one-fourth that for the all-BTE solver. Implementation of an algebraic multigrid solver is underway and is expected to significantly decrease computational time for the hybrid solver, and an asymptotic speed-up factor of about 16/3 is expected.

CONCLUSIONS

In this paper, the application of a hybrid Fourier-BTE solution algorithm to the problem of Joule heating in a bulk MOSFET has been described. The hybrid solver divides phonon groups by Knudsen number, solving those with low Knudsen numbers using a modified Fourier equation while those with high Kn are solved using a non-gray phonon BTE. The paper establishes that the hybrid solver produces computational results that are nearly indistinguishable from an all-BTE solution, and at significantly lower computational cost. It is suggested that further acceleration may be attained with a more efficient solution of the coupled Fourier and lattice temperature equations using an algebraic multigrid method in lieu of a line Gauss-Seidel algorithm.

The methodology holds promise for a variety of phonon transport problems in which the resolution of non-gray effects is critical. In superlattice transport, for example, interfaces between materials with significantly different acoustic properties imply that interfaces are transmissive only to select phonon modes. Similar considerations apply when considering thermal transport in composites. The hybrid model enables analysis of these complex physics at relatively low cost. Furthermore, the hybrid model may be extended to other classes of physics which employ governing equations similar to the BTE, for example in thermal radiation, neutron transport and in rarefied gas dynamics.

ACKNOWLEDGMENTS

We would like to thank Drs. Z. Aksamija and U. Ravaioli of UIUC for generously providing their e-MC data and Dr. Charles Ni for heat generation data. Support of J. Loy and J. Murthy by Purdue's PRISM Center under funding from the Department of Energy (National Nuclear Security Administration) Award Number DE-FC52-08NA28617 is gratefully acknowledged.

REFERENCES

- [1] International Technology Roadmap for Semiconductors (ITRS), [Online] 2002 <http://www.itrs.net/Links/2002Update/2002Update.pdf>.
- [2] Plumbridge, W. J., Matela, R. J., Westwater, A., 2004 "Structural Integrity and Reliability in Electronics." Kluwer Academic Publishers, Dordrecht
- [3] Rowlette, J. and Goodson, K. E., 2008, "Fully-Coupled Nonequilibrium Electron-Phonon Transport in Nanometer-Scale Silicon FETS." IEEE Transactions on Electron Devices, **55**(1) pp. 220-232
- [4] Pop, E., Dutton, R. W., Goodson, K. E., 2004, "Analytic Band Monte Carlo Model for Electron Transport in Si Including Acoustic and Optical Phonon Dispersion." Journal of Applied Physics, **96**(9)
- [5] Pop, E., Dutton, R. W. and Goodson, K. E., 2005, "Monte Carlo Simulations of Joule Heating in Bulk and Strained Silicon." Applied Physics Letters, **86**, 082191
- [6] Aksamija, Z. and Ravaioli, U., 2006, "Joule Heating and Phonon Transport in Silicon MOSFETS." Journal of Computational Electronics, **5**(4), pp. 431-434
- [7] Aksamija, Z. and Ravaioli, U., 2009, "Anharmonic Decay of Non-Equilibrium Intervalley Phonons in Silicon." Journal of Physics, **193**, 012033
- [8] Sinha, S., et al., 2005, "Scattering of g-Process Longitudinal Optical Phonons in Hotspots in Silicon." Journal of Applied Physics, **97**(2), pp. 023702-023709
- [9] Chen, G., 1997, "Size and Interface Effects on Thermal Conductivity of Superlattices of Periodic Thin-Film Structures." Journal of Heat Transfer, **119**, pp. 220-229
- [10] Sverdrup, P. G., Ju, Y. S. and Goodson, K. E., 2001, "Sub-Continuum Simulations of Heat Conduction in Silicon-on-Insulator Transistors." Journal of Heat Transfer, **123**, pp. 130-137
- [11] Narumanchi, S. V., Murthy, J. Y., and Amon, C. H., 2004, "Submicron Heat Transport Model in Silicon Accounting for Phonon Dispersion and Polarization." Journal of Heat Transfer **126**, pp. 946-955
- [12] Wang, T. J., 2007, "Sub-micron Thermal Transport in Ultra-scaled Metal Oxide Semiconductor (MOS) Devices." Ph. D. thesis, Purdue University, West Lafayette, IN.
- [13] Ni, C. and Murthy, J. Y., 2009, "Improved Phonon Transport Modeling Using Boltzmann Transport Equation with Anisotropic Relaxation Times." IPACK2009-89181, Proc. Of InterPACK. San Francisco, CA

- [14] Ni, C. and Murthy, J. Y., 2009, "Coupled Electro-Thermal Simulation of MOSFETS." IPACK2009-89182, Proc. Of InterPACK, San Francisco, CA
- [15] Sinha, S., Pop, E. and Goodson, K. E., 2006, "Non-Equilibrium Phonon Distributions in Sub-100 nm Silicon Transistors." *Journal of Heat Transfer*, **128**, pp. 638-647
- [16] Raithby, G. D. and Chui, E. H., 1992, "Implicit Solution Scheme to Improve Convergence Rate in Radiative Transfer Problems." *Numerical Heat Transfer*, **22**(3), pp. 251-272
- [17] Murthy, J. Y., Mathur, S. R., 1999, "Coupled Ordinate Method for Multi-Grid Acceleration of Radiation Calculations." *Journal of Thermophysics and Heat Transfer*, **13**(4), pp. 467-473
- [18] Chen, G., Henry, A. S., 2008, "Spectral Phonon Transport Properties of Silicon Based on Molecular Dynamics Simulations and Lattice Dynamics, *Journal of Computational and Theoretical Nanoscience*, **5**(2), pp. 1-12
- [19] Pascual-Gutierrez, J. A., Murthy, J. Y. and Viskanta, R. V., 2009, "Thermal Conductivity and Phonon Transport Properties of Silicon Using Perturbation Theory and the Environment-Dependent Interatomic Potential." *Journal of Applied Physics*, **106**, 063532
- [20] Jessee, J. P., Fiveland W. A., 1996, "Acceleration Schemes for the Discrete Ordinates Method." *Journal of Thermophysics and Heat Transfer*, **10**(3), pp. 445-451.
- [21] Hassanzadeh, P., 2007, "An Efficient Computational Method for Thermal Radiation in Participating Media." MASC thesis, University of Waterloo, Waterloo, Ontario.
- [22] Mathur, S. R. and Murthy, J. Y., 2009, "An Acceleration Technique for the Computation of Participating Radiative Heat Transfer." IMECE2009-12923, Proc. Of IMECE, Lake Buena Vista, FL
- [23] Lewis, E. and Miller, W., 1984, *Computational Methods of Neutron Transport*, John Wiley and Sons, New York, NY
- [24] Loy, J. M., Singh, D., Murthy, J. Y., 2009, "Non-gray Phonon Transport Using a Hybrid BTE-Fourier Solver." HT2009-88056, Proceedings of SHTC, San Francisco, CA
- [25] Bazant, M. Z., Kaxiras, E., and Justo, J. F., 1997, "Environment Dependent Interatomic Potential for Bulk Silicon." *Physical Review B*, **56**, pp. 8542-8552
- [26] Pascual-Gutierrez, J. A., Murthy, J. Y. and Viskanta, R. V., 2007, "Limits of Size Confinement in Silicon Thin Films and Wires." *Journal of Applied Physics*, **102**, pp. 034315
- [27] Murthy, J. Y., Mathur, S. R., "An Improved Computational Procedure for Sub-micron Conduction." *Journal of Heat Transfer*, **125**(5), pp. 904-911
- [28] Kittel, C., 1996, *Introduction to Solid State Physics*, Wiley, New York, NY
- [29] Ni, C., 2009, "Phonon Transport Models for Heat Conduction in Sub-Micron Geometries with Applications to Microelectronics." Ph. D. thesis, Purdue University, West Lafayette, IN
- [30] Mathur, S. R., Murthy, J. Y., 2002, "Computation of Sub-Micron Thermal Transport Using an Unstructured Finite Volume Method." *Journal of Heat Transfer*, **124**, pp. 1176-1184
- [31] Patankar, S. V., 1980, *Numerical Heat Transfer and Fluid Flow*, Taylor & Francis, London, England
- [32] Mingo, N., et al., 2003, "Predicting the thermal conductivity of Si and Ge nanowires." *Nano Letters* **3**(12), pp. 1713-1716
- [33] Akshaija, Z., Ravaioli, U., 2008, "Full-band Monte Carlo Simulation of Silicon Devices Including the Full Phonon Dispersion" to be Submitted to *Journal of Applied Physics* (2008)
- [34] Klemens, P. G., [ed.] F. Seitz and D. Turnbull, 1958, *Solid State Physics*, Academic Press, New York, NY
- [35] Briggs, W. L., Henson, V. E., and McCormick, S. F., 2000, *A Multigrid Tutorial*, SIAM, Philadelphia, PA

